Thin Solid Films 518 (2010) 5349–5354

Contents lists available at ScienceDirect

Thin Solid Films

journal homepage: www.elsevier.com/locate/tsf

Influence of microstructure and hydrogen concentration on amorphous silicon crystallization

N. Budini [a,*], P.A. Rinaldi [a], J.A. Schmidt [a,b], R.D. Arce [a,b], R.H. Buitrago [a,b]

[a] Instituto de Desarrollo Tecnológico para la Industria Química, UNL-CONICET, Güemes 3450, S3000GLN Santa Fe, Argentina
[b] Facultad de Ingeniería Química, UNL, Santiago del Estero 2829, S3000AOM Santa Fe, Argentina

ARTICLE INFO

Article history:
Received 26 August 2009
Received in revised form 23 March 2010
Accepted 10 April 2010
Available online 18 April 2010

Keywords:
Polycrystalline silicon
Hydrogenated amorphous silicon
Solid phase crystallization

ABSTRACT

Hydrogenated amorphous silicon samples were deposited on glass substrates at different temperatures by high frequency plasma-enhanced chemical vapor deposition. In this way, samples with different hydrogen concentrations and structures were obtained. The transition from an amorphous to a crystalline material, induced by a four-step thermal annealing sequence, has been followed. Effusion of hydrogen from the films plays an important role in the nucleation and growth mechanisms of crystalline silicon grains. Measurements of hydrogen concentrations, Raman scattering, X-ray diffraction and UV reflectance showed that an enhanced crystallization was obtained on samples deposited at lower substrate temperatures. A correlation between these measurements allows to analyze the evolution of structural properties of the samples. The presence of voids in the material, related to disorder in the amorphous matrix, results in a better quality of the resulting nanocrystalline silicon thin films.

1. Introduction

Crystalline silicon thin films have gained considerable attention in the last years on the basis of its potential applications to large area electronic devices, such as active-matrix liquid crystal displays, thin film transistors and solar cells [1]. In order to make the films competitive for these applications, different requirements have to be fulfilled. Among them, crystalline quality and grain size constitute some of the most important parameters.

Hydrogenated amorphous silicon (a-Si:H) deposited by plasma-enhanced chemical vapor deposition (PECVD) shows up as a relatively inexpensive and practical starting material for the development of large area crystalline silicon platforms. Several processes have been proposed in order to crystallize the a-Si:H in the most efficient way. The commonest and easiest method to achieve crystallization of a-Si:H is the solid phase crystallization (SPC), which can be yielded by conventional furnace annealing (CFA) [2]. Other available methods are excimer laser annealing (ELA) [3] and metal induced crystallization (MIC) [4]. ELA requires high production costs while MIC, which has been intensively investigated lately, involves an additional step — the deposition of the inducer — prior to the annealing. As in any conversion process of this kind, the final product is strongly related to the raw (as-deposited) material. Starting from amorphous silicon (a-Si) deposited by evaporation, Song et al. obtained a polycrystalline material with grain sizes up to 1.5 μm by CFA at 600 °C [5]. Depositing a-Si by high temperature PECVD, Matsuyama et al. obtained columnar grains of length up to 5 μm [6]. A stepwise annealing process on sputter-deposited a-Si:H films allowed Rüther et al. to obtain grain sizes as large as 10 μm [7].

Hydrogen incorporation during the deposition of a-Si:H by low temperature PECVD plays a key role in the internal structure of the films [8]. The crystallization process is influenced by the deposition temperature, which remarkably affects the hydrogen concentration, the film density and the amount of voids in the starting material [9]. Both dangling bonds and structural disorder are increased by lowering the substrate temperature and increasing the deposition rate [10]. Nucleation rate is also considered to be strongly related to structural defects. Moreover, it has been shown that the presence of voids in the precursor material may lead to a quicker crystallization [7,11]. Besides this, several authors [12–15] have pointed out the importance of hydrogen presence in the crystallization process, while the detailed mechanism remains still elusive [13].

Godet et al. have shown that mobile H atoms promote the formation of nanovoids and undercoordinated Si atoms in a step towards the crystallization of a-Si:H [12]. Kim et al. suggested that chemical annealing made with hydrogen plasma on a-Si samples is a very effective method in enhancing the grain growth rate [15], and Street has proposed that hydrogen, during the PECVD process, interacts with Si–Si bonds and induces a transition from amorphous to crystalline silicon [16].

In this work, the changes induced by CFA on structural properties of intrinsic a-Si:H, during the crystallization process, are investigated. For this purpose, a set of samples deposited at different temperatures were prepared at high growth rates by high frequency PECVD. Characterization techniques, like infrared transmittance, UV specular

* Corresponding author.
E-mail address: nbudini@intec.unl.edu.ar (N. Budini).

0040-6090/$ – see front matter © 2010 Elsevier B.V. All rights reserved.
doi:10.1016/j.tsf.2010.04.029

reflectance, Raman scattering and X-rays diffraction, were used in order to get an insight of the structural evolution of the samples. The role of void formation as well as the hydrogen effusion in the crystallization process is discussed.

2. Experimental details

Five samples were deposited on Schott AF-37 glass in a capacitively coupled PECVD reactor operating at a high frequency of 50 MHz and a power density of 120 mW/cm^2. Pure silane (SiH_4) was used as the reactant gas. The substrate temperature (T_s) was chosen to be 150, 200, 250, 300 and 350 °C for each sample. All samples were deposited at a pressure of 60 Pa. Due to the elevated frequency, deposition rates between 6 and 21 Å/s have been reached, leading to film thicknesses in the range of 0.9–3.7 μm. Each deposition was made also on single crystalline silicon (c-Si), as a reference for infrared measurements of hydrogen concentrations (C_H). Film thicknesses and optical band gaps were determined by optical interferometry following the analysis of Swanepoel [17].

The thermal annealing was performed in a tubular furnace with a constant flux of nitrogen at atmospheric pressure. To study the structural evolution of the films, from the amorphous (as-deposited) state to the microcrystalline state, the following thermal process was carried on: (i) 4 h at 400 °C (for dehydrogenation), (ii) plus 4 h at 500 °C, (iii) plus 4 h at 600 °C, and (iv) plus 4 h at 650 °C. The heating rate was always kept at 1 K/min. After each stage was completed, the samples were taken out of the furnace for characterization. The films deposited on c-Si were annealed together with the rest of the samples to follow the evolution of C_H.

Characterization involved infrared transmittance, UV specular reflectance, Raman scattering and X-ray diffraction measurements. Infrared transmittance was measured in a Perkin-Elmer Spectrum RX-FTIR System. UV specular reflectance was performed in a 330 Hitachi-Perkin-Elmer spectrometer, using a reflectance accessory that allows achieving low angle incidence conditions. Raman measurements were done with a Dilor spectrometer operating with the 632.8 nm line of a He–Ne laser allowing a maximum power density of ~730 kW/cm^2. The scattered Raman signal was integrated during 300 s for each spectrum. To assure that no local crystallization was being induced by the laser, successive spectra were obtained to see the evolution of the signal. X-ray diffraction was carried on in a Shimadzu XD-D1 diffractometer operating with the Cu Kα line (at 30 kV and 40 mA) in a θ–2θ drive configuration.

3. Results and discussion

Table 1 summarizes the deposition parameters of the samples together with the corresponding thicknesses and optical gaps determined by optical interferometry. Fig. 1 (solid line) presents the as-deposited infrared transmittance spectra of the sample deposited at $T_s = 200$ °C and its evolution with consecutive annealings. The different characteristic absorption bands of Si–H_n hydrides species ($n = 1, 2, 3$) can be clearly seen. The hydrogen concentrations of the samples were calculated by integration of the infrared absorption

Table 1
Measured and calculated parameters of as-deposited samples.

T_s (°C)	Deposition rate (Å/s)	Thickness (μm)	Optical gap (eV)
150	16	0.9	1.86
200	21	3.7	1.73
250	11	2.0	1.67
300	6	1.1	1.69
350	6	0.9	1.66

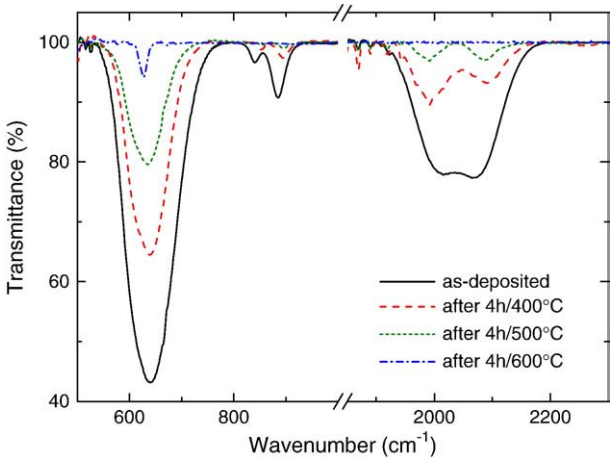

Fig. 1. Evolution of the infrared transmittance spectrum with different annealing steps for the sample deposited at $T_s = 200$ °C. A small amount of hydrides species still remains after 4 h at 600 °C, which is due to the elevated initial hydrogen concentration present in this sample.

band at 640 cm^{-1}, corresponding to the wagging oscillation mode of Si–H_n bindings. The expression

$$C_H = A\int \frac{\alpha(\omega)}{\omega} d\omega \tag{1}$$

was used, where the proportionality constant was taken to be $A = 2.1 \times 10^{19}$ cm^{-2} (see Ref. [18]). It has been shown that as C_H increases, a greater fraction of hydrogen is incorporated in the a-Si matrix forming clusters in the inner surface of micro-voids [8,19]. The remaining fraction is spread all over the material in a distributed or isolated phase. The relation between these two phases can be thought as the grade of structural disorder in the samples. In this sense, more disorder indicates a greater amount of voids in the material. The microstructure parameter, defined as

$$R^* = \frac{I_{2100}}{I_{2000} + I_{2100}} \tag{2}$$

quantifies roughly the fraction of clustered hydrogen present in the sample [8]. Here, I_{2000} and I_{2100} are the integrated infrared absorption bands at 2000 and 2100 cm^{-1}, respectively. The origin of these modes is generally assigned as follows. The 2000 cm^{-1} mode is attributed to the stretching oscillations of isolated Si–H bonds, while the 2100 cm^{-1} mode accounts for di- and tri-hydrides. However, monohydride groups bonded to silicon inside voids seem to contribute to this mode as well [20]. Thus, in any case, the 2100 cm^{-1} band accounts for a deviation from an ideal a-Si:H structure. The microstructure parameter is widely used to characterize the microstructure quality of a-Si:H [8,21].

In Fig. 2 (a) and (b) the dependence of C_H and R^* with deposition temperature T_s is shown. As can be seen, the initial H concentration increases as T_s decreases. This is in accordance with existing knowledge about a-Si:H obtained by PECVD, although at the commonly used lower frequency of 13.56 MHz [22,23]. The microstructure parameter indicates that the films also appear to contain a greater fraction of clustered hydrogen — hence to be more disordered — at lower values of T_s (Fig. 2 (b)). The density of a-Si:H obtained by PECVD decreases with C_H for percentages above 6–8 at.% [24,25].

The calculations of the microstructure parameter reveal, at the same time, that for samples with values of C_H greater than 8 at.% the fraction of clustered hydrogen increases abruptly from ~0.15 to ~0.50. These values may indicate an important presence of voids into the amorphous structure of the samples, deposited at high rates at temperatures below 250 °C.

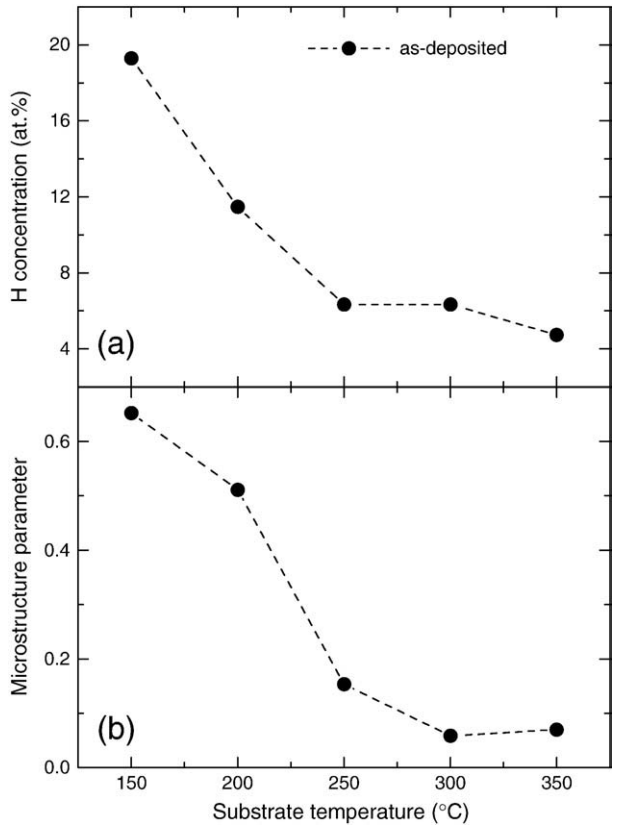

Fig. 2. Hydrogen concentrations (a) and calculated microstructure parameters (b) of the as-deposited samples as a function of T_s. The microstructure parameter was calculated from the corresponding integrated absorption bands (at 2000 and 2100 cm^{-1}) of infrared transmittance spectra and quantifies the amount of clustered H. Both quantities show the same trend, decreasing as T_s increases.

In Ref. [8] it has been shown that, independently of C_H, the concentration of isolated hydrogen does not exceed 4 at.%. Even more, clustered H predominates for C_H values higher than 10 at.%. These results agree with the observed tendency of the microstructure parameter in our samples.

From infrared spectra it is possible to calculate the relation of heights between the absorption peaks at 2000 and 640 cm^{-1}. This quotient measures the fraction of H bonded as monohydrides. Typical values for this parameter in a-Si:H grown at the standard frequency of 13.56 MHz lay in a particular range between 0.45 and 0.66 [21,26]. Fig. 3 shows a comparison of samples used in this work with those from other works. Similar values are seen for low C_H. For percentages above 8 at.% the proportion of monohydrides decreases considerably in these samples.

After the first stage of annealing, during 4 h at 400 °C for dehydrogenation, C_H diminishes considerably to values below 5 at.% in all samples, as shown in Fig. 4. As a consequence of this treatment, the sample deposited at $T_s = 150$ °C was severely damaged due to a violent dehydrogenation caused by high values of C_H. Reflectance measurements do not show any changes between the as-deposited state and after this first annealing. Also, the reflectance in the as-deposited state is the same for all samples. At the same time, Raman spectroscopy and X-ray diffraction do not distinguish any structural changes in the samples.

During the second stage of annealing, at 500 °C, hydrogen still effuses from the samples. At the end of this stage, no signal of Si–H infrared absorption was detected for higher T_s samples, while a small remanent percentage (<2 at.%) was observed for $T_s = 250$ and 200 °C samples. It is interesting to note that after 4 h at 500 °C some H remains into the samples deposited at lower temperatures. Infrared spectra

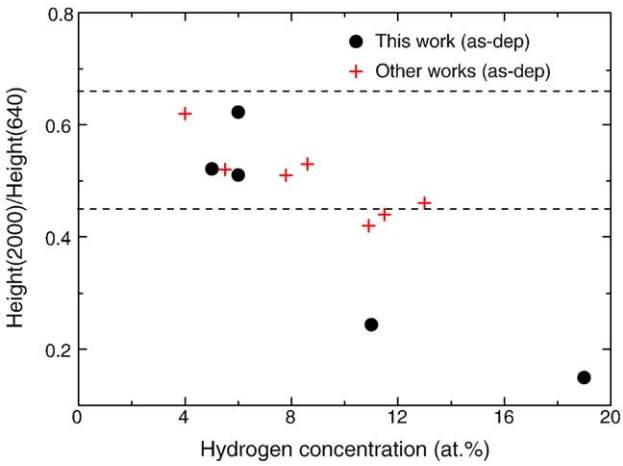

Fig. 3. Comparison of the ratio of heights of the 2000 and 640 cm^{-1} absorption bands between samples deposited in this work and samples deposited by the same method at lower RF frequencies. Typical values for samples deposited at 13.56 MHz are enclosed between dashed horizontal lines (see Refs. [21] and [26]).

showed that the 2100 cm^{-1} absorption band is still present (in a considerable proportion) in the sample deposited at $T_s = 200$ °C (see Fig. 1), which should account only for monohydrides located in voids since the effusion temperature of dihydrides occurs below 500 °C [11,27,28]. The calculated value of the R^* parameter for this sample (~0.4) reveals that still a considerable amount of H is bonded in clusters.

After the 500 °C annealing stage, again, neither X-ray diffraction nor Raman spectra show signs of crystallization. However, it is possible to detect subtle changes in the UV reflectance spectra of these samples, as can be observed in Fig. 5. This figure presents, in the first place, the spectrum of a polished single crystalline silicon wafer (thin solid line). This spectrum is characterized by two prominent peaks, located at ~275 and ~360 nm, corresponding to the optical interband transitions at the X point and along the Γ–L axis of the Brillouin zone, respectively [29]. The thick solid line corresponds to the spectrum of the samples in the as-deposited (amorphous) state. All the as-deposited samples exhibit the same spectrum within the experimental error, where no peak can be observed due to the lack of long-range order of the amorphous material. Although the spectra of the annealed samples do not show any noticeable peaks, they also differ from the spectrum of the amorphous samples. All the spectra approach that of c-Si in the region from 400 to 500 nm, excluding the possibility of the presence of a foreign film on the surface. The lower T_s samples show the most important changes, especially in the range of lower wavelengths. The decrease in specular

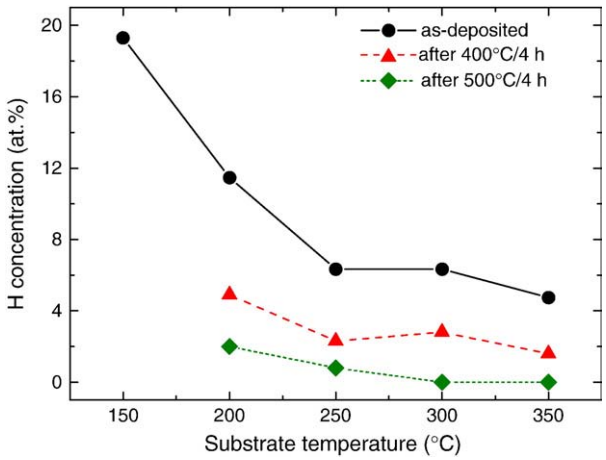

Fig. 4. Evolution of C_H with the annealing sequence. After 4 h at 500 °C there is no remaining hydrogen for the samples deposited at the two higher substrate temperatures.

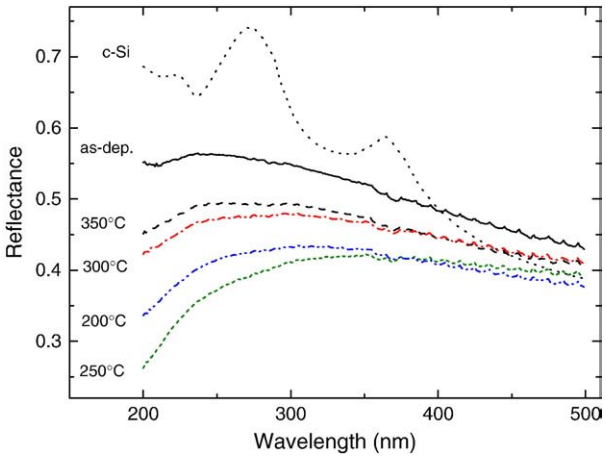

Fig. 5. Reflectance of the samples after the annealing step at 500 °C during 4 h. Differences from amorphous spectrum are seen, particularly for lower T_s samples.

reflectance in this wavelength range is typical of Rayleigh scattering caused by surface roughness, which increases as λ^{-4} (provided the vertical rms roughness of the scattering surface is much smaller than the wavelength of the incident light) [29]. The increase in surface roughness may be indicative of structural changes that are taking place as a consequence of the start-up of the crystallization process. This is a remarkable result due to the fact that UV reflectance seems to be sensitive to macroscopic structural changes to which Raman and X-ray diffraction are not.

Subsequently, samples were annealed during 4 h at 600 °C. This is the temperature at which a-Si starts to crystallize [30]. No hydrogen was detected in the samples by infrared transmittance after this annealing, except for a small amount remaining as monohydrides in the $T_s = 200$ °C sample as can be seen in Fig. 1. The resulting UV reflectance and X-ray diffraction spectra are shown in Fig. 6 (a) and (b), respectively. These spectra evidence that the crystallization process has taken place, especially for the samples deposited at the lower temperatures.

X-ray diffraction measurements show that the samples deposited at the lower T_s exhibit no sign of an amorphous phase. The intensity of the (1 1 1) peak was normalized to account for sample thickness, and the spectra are vertically displaced for clarity. On the other hand, the sample deposited at $T_s = 350$ °C shows no important changes in reflectance between the 500 and 600 °C annealing stages, while its X-ray spectrum is typically that corresponding to an amorphous sample. For the samples showing signs of crystallization, the ratio between the intensities of the (2 2 0) and (1 1 1) peaks differs from that reported for silicon powder [31,32], revealing a <1 1 1> preferred orientation.

An estimation of the grain size is possible from X-ray spectra of Fig. 6 (b) by means of Scherrer's formula

$$L = \frac{0.9\lambda}{\omega_{1/2}\cos\theta}, \tag{3}$$

where λ is the X-rays wavelength (0.154 nm in this case), $\omega_{1/2}$ is the peak width at half-maximum (in radians) and θ is half the angle in 2θ of the corresponding peak. A large-grained polycrystalline sample was used as a reference for the determination of the instrumental broadening. The calculations yield a grain size in the range of 24–28 nm for the $T_s = 200$, 250 and 300 °C samples, which allows asserting the nanocrystalline nature of the resulting films.

From an analysis of the peak heights of the reflectance spectra it is possible to estimate the crystallinity fraction and the crystalline quality of the samples [33,34]. Crystallinity fraction can be related to the quotient

$$\frac{\Delta R}{\Delta R_{c-Si}} = \frac{R_1 - R_2}{R_1^{c-Si} - R_2^{c-Si}}, \tag{4}$$

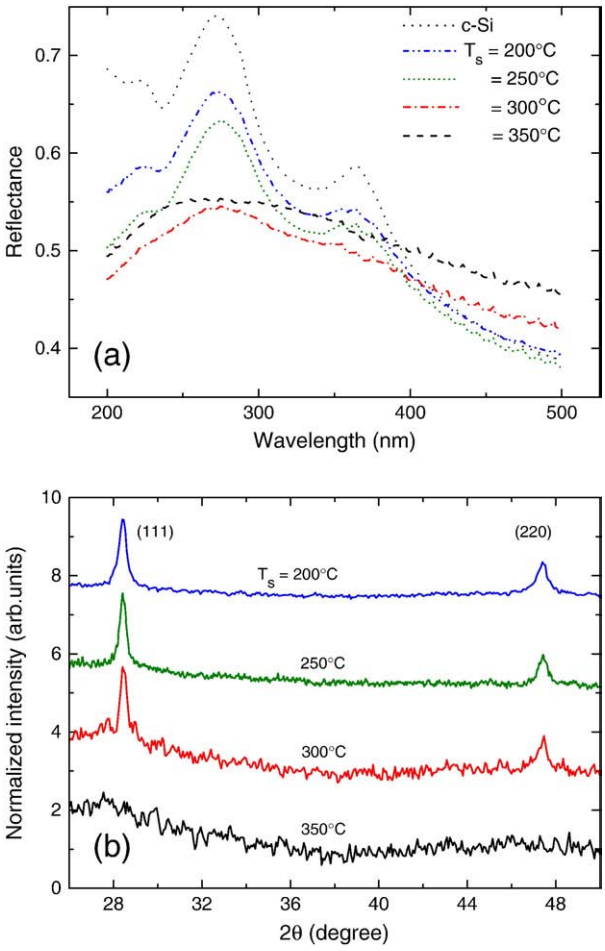

Fig. 6. UV specular reflectance (a) and X-ray diffraction (b) spectra of the samples after the annealing stage at 600 °C during 4 h. Evidence of crystallization is seen for all substrate temperatures, except for the 350 °C one.

where R_1 and R_2 are the measured reflectances at $\lambda = 275$ and 365 nm, and the superscript "c-Si" refers to the known values of single crystalline silicon. According to Ref. [33], the definition of ΔR is based on the fact that the 275 nm peak intensity is influenced by crystallinity and also by surface roughness while the 365 nm one accounts mainly for roughness. On the other hand, the crystalline quality factor, Q, is defined as [34]

$$Q = \frac{1}{2}\left[\frac{R_1}{R_1^{c-Si}} + \frac{R_2}{R_2^{c-Si}}\right]. \tag{5}$$

As can be seen in Ref. [34], this factor quantifies how similar to single crystalline silicon is the spectrum of each sample.

Calculated values for the ΔR and Q parameters, after the 600 °C annealing step, are shown in Table 2. For the highest T_s sample it was impossible to calculate them since no peaks were present in the corresponding reflectance spectrum.

As a final step, samples were annealed at 650 °C during 4 h. After this, crystalline signs can be seen in all samples, as shown in Fig. 7 which presents results from Raman spectroscopy. The typical crystalline silicon peak at ~520 cm^{-1} is present and indicates that crystallization has evolved in the whole set of samples.

In order to roughly determine the crystalline fraction of the films from Raman spectra, a deconvolution procedure was performed. The fitting process involved the following functions: a linear background, a Lorentzian peak around 520 cm^{-1} corresponding to the TO phonon mode of c-Si, and two Gaussian peaks corresponding to contributions

Table 2
Calculated crystallinity parameters from UV reflectance (Q and ΔR) after the 600 °C annealing step and from Raman spectroscopy (X_c) after the 650 °C annealing step. For $T_s = 350$ °C the parameters Q and ΔR could not be calculated.

T_s (°C)	Q	ΔR	X_c
200	0.91	0.81	0.95
250	0.88	0.71	0.97
300	0.79	0.31	0.90
350	–	–	0.84

from amorphous (TO mode) and fine crystalline (or grain boundaries) phases centered at 480 and 500 cm^{-1}, respectively [35]. A detail of the fitting is shown in the inset of Fig. 7. The crystalline fraction can be estimated as

$$X_c = \frac{(A_{500} + A_{520})}{(\alpha A_{480} + A_{500} + A_{520})}, \quad (6)$$

where A_x is the integrated area of each peak and the factor $\alpha = 0.8$ takes account of the higher phonon excitation cross-section of a-Si [35].

The calculated values of X_c are shown in Fig. 8 (stars), together with the obtained values for the full width at half-maximum (FWHM) of the c-Si Lorentzian peak at 520 cm^{-1} (diamonds), and the quotient A_{500}/A_{all} (circles), where A_{500} is the area of the 500 cm^{-1} peak (fine crystalline phase) and A_{all} is the integrated area of all the peaks. A maximum X_c of 97% was obtained for the $T_s = 250$ °C sample, in agreement with a minimum FWHM of 6.7 cm^{-1} and a minimum in the fine crystalline phase. The decrease of X_c for higher and lower deposition temperatures is also followed by an increase of FWHM and A_{500}/A_{all}, showing a close correlation between these parameters.

Kim et al. reported that signs of crystallization are detected in Raman spectra only after a 12 h annealing at 600 °C (in PECVD a-Si:H samples deposited from hydrogen diluted silane) [11]. However, in this work crystalline signals are already detected after only 4 h at 600 °C. From the analysis of the results of UV reflectance and Raman spectroscopy, it is possible to conclude that samples deposited at lower temperatures have a higher crystallinity than those deposited at higher temperatures. As can be seen in Table 1, the thickness of the samples (those that crystallize without peeling off) decreases from 3.7 μm for $T_s = 200$ °C to 0.9 μm for $T_s = 350$ °C. One would expect the thinner samples to crystallize first; however, that is not the case. The

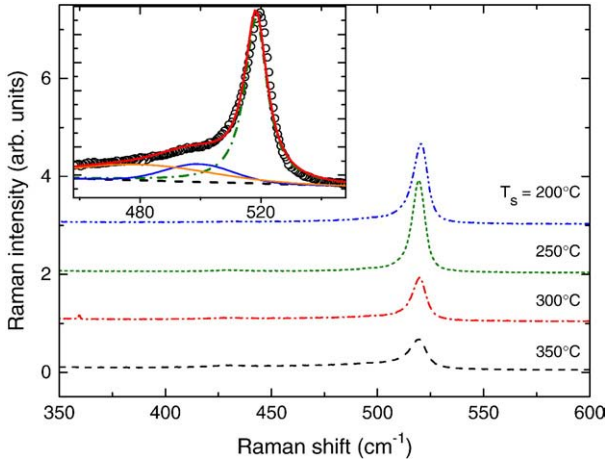

Fig. 7. Raman scattering spectra of samples after the last annealing step at 650 °C during 4 h. Crystalline peaks are observed, also in the $T_s = 350$ °C sample, which did not show crystalline signals in X-ray diffraction and UV reflectance spectra in the preceding steps. The inset shows the functions used in the fitting procedure: a linear background (dashed line), a Lorentzian peak at 520 cm^{-1} (dash-dotted line), and two Gaussian peaks at 500 and 480 cm^{-1} (solid lines).

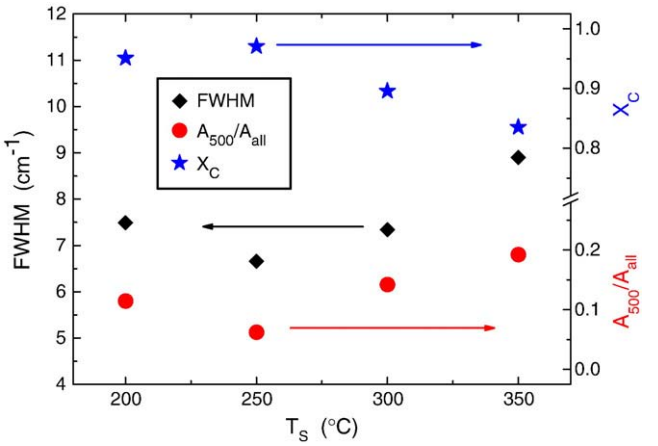

Fig. 8. Crystallinity related parameters, calculated from the fitting and deconvolution of the Raman spectra. The trends of the FWHM (black diamonds) and A_{500}/A_{all} (red circles) values are in agreement with that of the crystallinity fraction, X_c (blue stars).

samples that start to crystallize earlier and that attain the highest degree of crystallinity are those deposited at $T_s = 200$ and 250 °C. Therefore, a thickness-related effect on the crystallization can be ruled out.

Previous works have shown that a greater disorder in the precursor material retards nucleation and favors grain growth [7,11]. A consequence of this should be a larger resulting crystalline fraction. In this work, samples with a more disordered structure (i.e., containing a larger amount of voids), obtained at lower substrate temperatures, show a faster crystallization process, as observed in UV reflectance, X-rays diffraction and Raman spectra. However, structural disorder is not the only factor to be considered in the crystallization process. The amount of hydrogen is very high for samples deposited at lower temperatures. Also in the sample deposited at 350 °C the H concentration is still important. Therefore, the role of hydrogen effusion during the SPC process has to be considered.

Some authors claim that hydrogen alone can induce crystallization of the a-Si:H network [13]. Other studies suggest that in order to obtain microcrystalline silicon films, both hydrogen atoms and Si–H_n radicals must be present [12]. According to Godet et al., the trapping of a mobile H atom by a strong Si–H bond can produce a broken bond (trivalent Si atom) and a cluster of two Si–H bonds, forming a nanovoid (represented as SiH HSi), as expressed by the following reaction

$$\mathrm{SiHSi} + \mathrm{Si{-}H} \rightarrow \mathrm{Si^0} + \mathrm{SiHHSi}, \quad (7)$$

which describes why the formation of a Si–H_n phase appears to be a necessary step towards the crystallization [12]. This chemical reaction continues with Si–H bond breaking and recombination of atomic hydrogen to form H_2, providing the energy (chemical annealing) for the rearrangement of the silicon network, i.e., its crystallization [36]. The results obtained in this work can be interpreted within this model, considering that non-hydrogenated a-Si needs to be annealed at temperatures higher than 600 °C for more than 12 h to start the crystallization process. In the samples under study, instead, a higher C_H leads to a faster crystallization.

The presence of Si–H_n bonds leads to the production of atomic H during the SPC process. The interaction of H and Si–H bonds gives as a result minuscule crystallites in a very high density, in correspondence with the voids density. This process seems to start with the 500 °C annealing, as shown by the UV reflectance data of Fig. 5. These crystallites can act as seeds during the subsequent annealing at

600 °C, where they grow until collision with their neighbors. Hence, this leads to the formation of a nanocrystalline material, in accordance with the results obtained.

4. Conclusions

The crystallization of a-Si:H samples deposited by PECVD at different substrate temperatures and at high deposition rates has been studied. The evolution of the microstructure and its influence on the crystallization process has been followed. After a thermal treatment consisting of successive and isochronic stages of 4 h at 400, 500, 600 °C and 650 °C, the samples crystallized. Crystallization was checked by UV specular reflectance, Raman spectroscopy and X-ray diffraction measurements. An increasing crystalline fraction was detected for lower substrate temperatures. In particular, as is clearly seen in Raman results after the last annealing of 4 h at 650 °C, the sample deposited at 250 °C showed the highest crystalline fraction. It is concluded that the hydrogen effusion and the structural disorder strongly influence the crystallization process. High hydrogen concentrations lead to a high density of crystalline nuclei which prevent grains to grow to a considerable size, resulting in a nanocrystalline material with grain sizes in the range of 24–28 nm. Therefore, to obtain a larger grain size a different growing regime of the material should be used, leading to no H incorporation and a moderate-to-high degree of structural disorder. Ultra-high deposition rates at high temperatures would be suitable; however, this needs further research. An important result was obtained by UV reflectance, which detected the onset of crystallization after the annealing stage at 500 °C. This technique shows up as a sensitive method to reveal the early stages of crystallization, even before Raman scattering or X-ray diffraction detect any changes.

Acknowledgments

This work was supported by projects of the ANPCyT (PICT 25749) and CONICET (PIP 5246). We also acknowledge the support given by the Universidad Nacional del Litoral and by Dmitri Daineka from the Laboratoire de Physique des Interfaces et des Couches Minces (LPICM) of École Polytechnique at France.

References

[1] A.G. Aberle, Thin Solid Films 511/512 (2006) 26.
[2] R.B. Iverson, R. Reif, J. Appl. Phys. 62 (1987) 1675.
[3] G. Ivlev, E. Gatskevich, V. Cháb, J. Stuchlík, V. Vorlíček, J. Kočka, Appl. Phys. Lett. 75 (1999) 1498.
[4] S.Y. Yoon, S.J. Park, K.H. Kim, J. Jang, Thin Solid Films 383 (2001) 34.
[5] D. Song, D. Inns, A. Straub, M.L. Terry, P. Campbell, A.G. Aberle, Thin Solid Films 513 (2006) 356.
[6] T. Matsuyama, N. Nerada, T. Baba, T. Sawada, S. Tsuge, K. Wakisaka, S. Tsuda, J. Non-Cryst. Solids 198/200 (1996) 940.
[7] R. Rüther, J. Livingstone, N. Dytlewski, Thin Solid Films 310 (1997) 67.
[8] J.D. Ouwens, R.E.I. Schropp, Phys. Rev. B 54 (1996) 17759.
[9] W. Beyer, Sol. Energy Mater. Sol. Cells 78 (2003) 235.
[10] K. Nakazawa, K. Tanaka, J. Appl. Phys. 68 (1990) 1029.
[11] H. Kim, K. Lee, J. Lee, Thin Solids Films 302 (1997) 17.
[12] C. Godet, N. Layadi, P. Roca i Cabarrocas, Appl. Phys. Lett. 66 (1995) 3146.
[13] F. Kail, A. Hadjadj, P. Roca i Cabarrocas, Thin Solid Films 487 (2005) 126.
[14] S. Jia, H.C. Ge, X.H. Geng, Z.P. Wang, Sol. Energy Mater. Sol. Cells 62 (2000) 201.
[15] H.Y. Kim, Y.S. Kang, P.S. Lee, J.Y. Lee, Thin Solid Films 402 (2002) 296.
[16] R. Street, Phys. Rev. B 43 (1991) 2454.
[17] R. Swanepoel, J. Phys. E: Sci. Instrum. 16 (1983) 1214.
[18] M.H. Brodsky, M. Cardona, J.J. Cuomo, Phys. Rev. B 16 (1977) 3556.
[19] D.L. Young, P. Stradins, Y. Xu, L.M. Gedvilas, E. Iwaniczko, Y. Yan, H.M. Branz, Q. Wang, Appl. Phys. Lett. 90 (2007) 081923.
[20] A.H.M. Smets, W.M.M. Kessels, M.C.M. van de Sanden, Appl. Phys. Lett. 82 (2003) 1547.
[21] W. Beyer, M.S. Abo Ghazala, Mater. Res. Soc. Symp. Proc. 507 (1998) 601.
[22] A.H. Mahan, J. Carapella, B.P. Nelson, R.S. Crandall, I. Balberg, J. Appl. Phys. 69 (1991) 6728.
[23] S. Ray, S. Mukhopadhyay, T. Jana, R. Carius, J. Non-Cryst. Solids 299 (2002) 761.
[24] X. Jiang, B. Goranchev, K. Schmidt, P. Grünberg, K. Reichelt, J. Appl. Phys. 90 (1990) 6772.
[25] C.R. Miranda, K.V. Tretiakov, S. Scandolo, J. Non-Cryst. Solids 352 (2006) 4283.
[26] A.H. Mahan, L.M. Gedvilas, J.D. Webb, J. Appl. Phys. 87 (2000) 1650.
[27] J.A. Mcmillan, E.M. Peterson, J. Appl. Phys. 50 (1979) 5283.
[28] A.H. Mahan, B. Roy, R.C. Reedy Jr., D.W. Readey, D.S. Ginley, J. Appl. Phys. 99 (2006) 023507.
[29] G. Harbeke, L. Jastrzebski, J. Electrochem. Soc. 137 (1990) 696.
[30] J. Robertson, J. Appl. Phys. 87 (2000) 2608.
[31] S.Y. Yoon, S.J. Park, K.H. Kim, J. Jang, C.O. Kim, J. Appl. Phys. 87 (2000) 609.
[32] J.A. Schmidt, N. Budini, P.A. Rinaldi, R.D. Arce, R.H. Buitrago, J. Cryst. Growth 311 (2008) 54.
[33] G.W. Cullen, M.S. Abrahams, J.F. Corboy, M.T. Duffy, W.E. Ham, L. Jastrzebski, R.T. Smith, M. Blumenfeld, G. Harbeke, J. Lagowski, J. Cryst. Growth 56 (1982) 281.
[34] A. Straub, P.I. Widenborg, A. Sproul, Y. Huang, N. Harder, A.G. Aberle, J. Cryst. Growth 265 (2004) 168.
[35] C. Becker, F. Ruske, T. Sontheimer, B. Gorka, U. Bloeck, S. Gall, B. Rech, J. Appl. Phys. 106 (2009) 084506.
[36] A. Fontcuberta i Morral, P. Roca i Cabarrocas, J. Non-Cryst. Solids 299/302 (2002) 196.